



# Glucose Sensing Mediated by Portal Glucagon-Like Peptide 1 Receptor Is Markedly Impaired in Insulin-Resistant Obese Animals

Charles-Henri Malbert,<sup>1</sup> Alain Chauvin,<sup>2</sup> Michael Horowitz,<sup>3</sup> and Karen L. Jones<sup>3</sup>

*Diabetes* 2021;70:99–110 | <https://doi.org/10.2337/db20-0361>

**The glucose portal sensor informs the brain of changes in glucose inflow through vagal afferents that require an activated glucagon-like peptide 1 receptor (GLP-1r). The GLP-1 system is known to be impaired in insulin-resistant conditions, and we sought to understand the consequences of GLP-1 resistance on glucose portal signaling. GLP-1-dependent portal glucose signaling was identified, in vivo, using a novel <sup>68</sup>Ga-labeled GLP-1r positron-emitting probe that supplied a quantitative in situ tridimensional representation of the portal sensor with specific reference to the receptor density expressed in binding potential units. It also served as a map for single-neuron electrophysiology driven by an image-based abdominal navigation. We determined that in insulin-resistant animals, portal vagal afferents failed to inhibit their spiking activity during glucose infusion, a GLP-1r-dependent function. This reflected a reduction in portal GLP-1r binding potential, particularly between the splenic vein and the entrance of the liver. We propose that insulin resistance, through a reduction in GLP-1r density, leads to functional portal desensitization with a consequent suppression of vagal sensitivity to portal glucose.**

The maintenance of plasma glucose homeostasis is dependent on the integration of glucose-sensing mechanisms located in the brain, portal vein, and intestine (1). The impact of obesity and insulin resistance on brain glucose sensing has been investigated extensively (2), but there is much less information about the hepatoportal sensor (3). Nevertheless, there is compelling evidence that the portal glucose sensor plays a pivotal role in glucose homeostasis (4,5). During hypoglycemic episodes induced by fasting or

iatrogenic insulin administration, the portal sensor elicits counterregulation to increase plasma glucose (6). A hepatoportal-to-brain sympathoadrenal neural network is responsible for this response (7). In contrast, vagally mediated information from the portal sensor is responsible for the regulatory response to portal hyperglycemia, including during the postprandial state (8,9). There is indirect evidence that a neuronal circuit responsible for regulatory response to portal hyperglycemia, including attenuation of portal glucose-stimulated insulin secretion by ganglionic blockade (8) and after surgical denervation of the liver and the portal vein area (10). Unfortunately, there is a lack of direct confirmation of portal-sensitive neurons, reflecting the sparsity of the portal innervation (11). Nijima and colleagues (12,13) described portal vagal afferents with both decreased and increased spiking during portal glucose infusion. Their recording, which represents the only direct measurement of portal vagal afferents, was made from bundles rather than from single fibers, and hence, the net result represents a summation of different fiber responses, some of which being excitatory and others inhibitory. Confounding these difficulties in identifying the portal sensor, there is evidence that the glucagon-like peptide 1 receptor (GLP-1r) is associated critically with portal glucose sensing (14). In particular, GLP-1r is expressed by vagal afferents in the wall of the hepatic portal vein (15), GLP-1 coinfusion is required for portal glucose to stimulate insulin response (8), coinfusion of glucose and a GLP-1r antagonist into the portal vein inhibits glucose clearance and increases glycemia transiently (16), and vagal GLP-1r knockdown blunts postprandial insulin release and increases glycemia (17).

<sup>1</sup>Aniscan Unit, Department of Human Nutrition, INRAE, Saint-Gilles, France

<sup>2</sup>UEPR Unit, Department of Animal Physiology, INRAE, Saint-Gilles, France

<sup>3</sup>Centre of Research Excellence in Translating Nutritional Science to Good Health, Adelaide Medical School, The University of Adelaide, Adelaide, South Australia, Australia

Corresponding author: Charles-Henri Malbert, [charles-henri.malbert@inrae.fr](mailto:charles-henri.malbert@inrae.fr)

Received 9 April 2020 and accepted 6 October 2020

This article contains supplementary material online at <https://doi.org/10.2337/figshare.13063706>.

© 2020 by the American Diabetes Association. Readers may use this article as long as the work is properly cited, the use is educational and not for profit, and the work is not altered. More information is available at <https://www.diabetesjournals.org/content/license>.

Collectively, the outcomes of these studies suggest that an impaired capacity of the portal vagal sensor to detect hyperglycemia, as a result of a defective GLP-1r system, is associated with insulin-resistant obesity. In contrast, using a sodium–glucose cotransporter 3 (SGLT3) agonist with glucose coinfusion in the portal vein, Pal et al. (3) reported a more pronounced glucose-lowering effect of portal glucose in anesthetized ZDF rats. Unlike the GLP-1-mediated response, the SGLT3-mediated response was resistant to acute subdiaphragmatic vagotomy.

Several lines of evidence indicate that the GLP-1 system is impaired in insulin-resistant individuals and that GLP-1 resistance may be fundamental to the pathophysiology of prediabetes (18). The latter phenomenon may be attributable, at least in part, to a reduction in GLP-1r density, but this has not been investigated in the portal region despite the established fundamental role of the GLP-1r in the function of the portal sensor (19). Irrespective of the difficulties inherent in the quantitative measurement of receptor density (20) together with the heterogeneous correlation of single-cell RNA sequencing and protein expression for a sparingly expressed receptor such as GLP-1r (21), Broide et al. (22) reported that GLP-1r expression in the gastric glands of individuals with type 2 diabetes is reduced. Similarly, in obesity-prone rats, impaired GLP-1 signaling observed within the nodose ganglia may exacerbate hyperphagia (23). A similar phenomenon might also exist at the portal sensor level and, if so, might be of importance to impaired glucose sensing in insulin-resistant obese subjects (24). The achievements of the Eriksson team in labeling the GLP-1r agonist with a positron emitter (25), while initially targeted toward detection of insulinomas, have provided the capacity to quantify GLP-1r noninvasively. This was made possible by the design of the extemporaneous synthesis sequence of a  $^{68}\text{Ga}$ -labeled Exendin-4 tracer and its companion quality control process (26). Aside from being minimally invasive and allowing longitudinal measurements, this technique, using positron-emitting imaging, supersedes nonquantitative histological techniques using suboptimal antibodies (27).

We proposed to quantify the GLP-1r within the portal vein sensor in normal and insulin-resistant obese animals. We also aimed to demonstrate that the changes in GLP-1r density identified by positron emission tomography (PET) imaging are functionally relevant. With use of the GLP-1r map as a reference for the surgical navigation system, vagal afferents were recorded *in vivo*, using the single-neuron method (28,29), while maintaining intact neuronal connections among the gut, the pancreas, and the brain. Vagal afferents originating from the GLP-1r-rich portal area were further identified using field stimulation and characterized by glucose infusion with and without GLP-1r antagonism. Since the relationship between vagal afferent discharge and the portal glucose concentration appeared nonlinear in rats (30), portal glucose concentrations were adapted to the endogenous glucose production rate measured during the postprandial state (31) (i.e., the

concentration likely encountered by the portal sensor). We performed our experiments in miniature obese and lean Yucatan adult pigs in part because of the higher spatial resolution, even when compared with that obtained in rats using a dedicated miniature PET imager (32). The size of the animal also allowed the implementation of surgical navigation with a millimetric intrinsic positioning error (33). Furthermore, extensive agonist displacement studies have been performed in this species to ascertain the specific binding of the radioactive probe (34). Finally, the miniature pig (mini-pig) is known to develop obesity and insulin resistance rapidly in response to a high-fat/sucrose diet (35).

## RESEARCH DESIGN AND METHODS

### Experimental Protocol

A total of 12 adult Yucatan mini-pigs (National Research Institute for Agriculture, Food, and Environment [INRAE]), matched for age and sex, were studied. At 1 year of age, six animals were fed a high-fat, high-sucrose diet (4,024 kcal/kg feed) supplied at 150% of the recommended caloric intake for 5 months to induce morbid obesity (31). The remaining six animals were maintained on a low-fat, low-sucrose diet (2,275 kcal/kg feed) for 5 months to limit body fat and ensure that total body weight was <40 kg. After this time and while animals were provided with the same feeding regimen, PET/computed tomography (CT) imaging of the portal area, using a GLP-1r PET radiotracer and radioopaque CT (injected images), were concurrently performed. Injected and noninjected CT images were used in conjunction with the PET image to locate the portal area with the maximal density of GLP-1r for the electrophysiological study. The noninjected CT scan was also used to evaluate the abdominal fat deposit. Insulin sensitivity was measured during the same anesthesia after completion of the imaging procedure by euglycemic-hyperinsulinemic clamp. Three to 4 weeks later, once the animals had resumed their feeding behavior, portal vagal afferent sensing was measured using the single afferent fiber method (36). In the interval between procedures, the animals were housed individually in 2-m<sup>2</sup> cages and enriched with toys to encourage physical exercise. Visual and limited physical contact between animals was permitted by the design of the cages. Animals were subsequently euthanized using T61 (Intervet, Beaucauzé, France) at the end of the electrophysiological procedure. The experiment was conducted according to the ethical standards of European and French legislation and with the approval of the Rennes Animal Ethics Committee (2018053109128366).

### PET GLP-1r Imaging and Image Analysis

GLP-1r was labeled with the use of [ $^{68}\text{Ga}$ ]Ga-DO3A-VS-Cys40-Exendin-4 produced onsite using an automated workflow (26) adapted for a scintomics radioactive synthesizer (37) (see Supplementary Material). PET images were acquired during isoflurane anesthesia using a Discovery ST PET-CT scanner (GE Healthcare, Belfort, France). Mini-pigs

were anesthetized with isoflurane (measured minimum alveolar concentration 1.8 vol) in an air/O<sub>2</sub> mixture. The ventilation parameters were set to maintain end-tidal carbon dioxide concentration at  $4.3 \pm 2\%$  and oxygen saturation as measured by pulse oximetry at  $\geq 98\%$ , while the insufflation pressure was  $< 20$  mmHg (ADU-AS/3; GE). Homeothermy was maintained using a forced-hot-air blanket (Bair Hugger; 3M, Cergy-Pontoise, France).

Immediately before imaging, access to arterial blood was achieved with a Seldinger-type catheter (RS+A50K10SQ; Terumo, Guyancourt, France) inserted extemporaneously under echographic guidance (M-Turbo; Sonosite, Paris, France) into either the left or the right femoral artery. A venous catheter was also placed in one of the saphenous veins contralateral to the arterial catheter. Three fiducial radio-opaque markers (1-mm metal spheres) were also placed using a permanent stitch on the skin of the animal to calibrate the surgical navigation used during the electrophysiological study.

Each animal was positioned to include the abdomen in the 15-cm axial field of view of a Discovery ST PET/CT scanner with the assistance of a low-dose CT scout view (140 kV, 10 mA). Attenuation correction was acquired with a CT examination at 140 kV and 10–80 mA. <sup>68</sup>Ga-DO3A-Exendin-4 (0.2 MBq/kg) was administered intravenously over 30 s using an automated injector, and animals were examined with a dynamic PET protocol for 60 min (30 frames; 12 \* 10 s, 6 \* 30 s, 5 \* 120 s, 5 \* 300 s, and 2 \* 600 s). Concurrent with the PET scanning, arterial blood radioactivity was recorded continuously using an inline device coupled with a  $\gamma$ -ray detector (Model 802 Canberra; Mirion Technologies [Canberra], Meriden, CT) placed on the external artery-venous loop. Composite arterial input function was built from these measurements using AniMate software (38).

Following the PET imaging, an injected CT sequence was initiated to obtain an accurate anatomical image of the portal vein that was difficult to delineate using the non-injected CT imaging in obese animals. Briefly, three high-speed imaging sequences were achieved at 30, 60, and 180 s after the intravenous administration of the contrast medium (Optiject 300 mg/mL, 100 mL, 4 mL/s; Guerbet, Aulnay-sous-Bois, France). These images were used to build a volume of interest (VOI) of the portal vein using ITK-SNAP software (Fig. 1A).

The GLP-1r binding potential (specific volume of distribution [V<sub>s</sub>]) was obtained using compartmental kinetic analysis (see Supplementary Material, Kinetic Analysis of [<sup>68</sup>Ga]Ga-DO3A-VS-Cys40-Exendin-4) of the radioactivity in the portal VOI together with the arterial input function after corrections for attenuation, scatter, dead time, and partial volume effect. PET images were reconstructed using an iterative ordered subset expectation maximization algorithm (three-dimensional iterative, 4-mm Hann filter, two iterations/21 subsets) into a 128 \* 128 matrix with pixel size 2.34 \* 2.34 \* 3.27 mm. Reconstructed data were analyzed using PMOD 3.9 software (PMOD, Zürich, Switzerland) that was also used for partial volume correction (39).

### Electrophysiology Acquisition and Analysis

The stimulating electrodes were connected to form electrode pairs each of  $< 800 \Omega$  impedance. The parameters used for afferent characterization (30 V, 2 Hz, 2 ms, 10-s trains) were adapted to stimulate unmyelinated fibers (40) since below the diaphragm, most neurons are classified as C or A $\delta$  (41,42). Once identified, the conduction speed was calculated, knowing the time of occurrence of the action potential and the distance between the stimulating and recording electrodes. The latter was calculated, with an  $\sim 5$ -mm error, using the CT images that incorporate the bottom part of the skull to image the nerve dissection area. The same laparoscopic abdominal access was used to insert a silicon catheter with its distal end located precisely at the center of the 40-mm portal segment under scrutiny.

Electrical activity from vagal afferent neurons was recorded using classical neurophysiological methods adapted to the pig (28,29,43). Glucose (20%) at 0.045 mL/kg/min was infused for 5 min into the portal catheter to quantify the portal sensor response. The amount of glucose infused corresponded to three times the endogenous glucose production rate in the fasted pig (31,44). Exendin-3 (9-39) (50 pmol/kg; Sigma, Lyon, France), an antagonist of the GLP-1r, was coinjected with glucose at the completion of the experiment to evaluate the involvement of the GLP-1r in the reduction in firing rate induced by portal glucose. The initial glucose infusion and the exendin-3 (9-39)/glucose coinjection were separated by 1 h. During this time, the neuron under scrutiny was unloaded from the recording electrode.

### Statistical Analysis

Data were analyzed using a two-tailed unpaired *t* test with GraphPad Prism 8 (GraphPad Software) and are presented as mean  $\pm$  SEM unless otherwise indicated. Differences were considered statistically significant if  $P \leq 0.05$ . Residuals were analyzed using quantile-quantile plot for normality.

### Data and Resource Availability

The data sets generated and analyzed during the current study are available from the corresponding author upon reasonable request. Imaging data and analysis of PET images are available as a single PMOD-compatible database. Electrophysiological data are available as individual Spike2 files.

## RESULTS

### Insulin Sensitivity and Body Composition

All animals in the obese group had an approximate doubling in body weight, primarily as a result of an increased abdominal fat mass that was about six times that of the lean animals. The abdominal fattening in part reflected an increase in visceral fat, but the major increase was in subcutaneous fat. Mean fasting plasma glycemia was slightly, but not significantly, increased in the obese compared with the lean group. The obese animals were

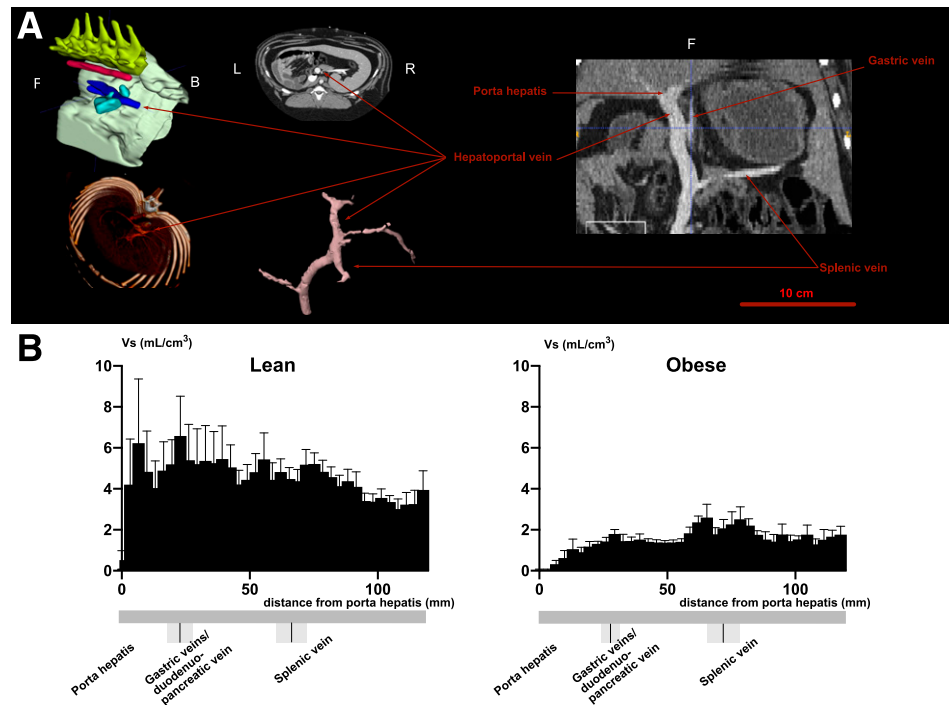


**Figure 1**—A: Contrast-enhanced CT images of the portal area in an adult mini-pig. The right side shows an image obtained 20 s post-contrast medium administration and used to identify the anatomical arrangement of the mesenteric, portal, splenic, and gastric veins. The duodenopancreatic vein is visible only in some animals (see Supplementary Fig. 6). The left side shows a three-dimensional reconstruction of the portal vein and its collaterals together with the extension of the extra- vs. intrahepatic portal vascular distribution. B: Distribution of GLP-1r density along the portal system obtained by pixelwise volumetric mean calculation from the Vs-coded PET image. Vs (for volume of the specifically bound compartment [see Supplementary Table 1]) quantifies GLP-1r density. The path of the portal vein was calculated using the contrast-enhanced CT image, and the resulting transformation matrix was applied to the Vs-coded PET image. In gray, below the histogram, the mean (black bar) and SE position (in gray; width = SE) of the gastric and splenic veins are presented relative to porta hepatis. The size of the horizontal gray bar, representing the portal vein, is not indicative of its actual width and has been inserted for depiction purposes only. B, back; F, front; L, left; R, right.

clearly insulin resistant on the basis of the euglycemic-hyperinsulinemic clamp. The calculated insulin sensitivity index was reduced by  $\sim 70\%$  compared with the lean group (Table 1).

#### GLP-1r Portal Distribution

$[^{68}\text{Ga}]\text{Ga-DO3A-VS-Cys40-Exendin-4}$  showed a recognizable uptake within the portal vein area. There was also significant uptake by the pancreas, which could be identified separately from the portal area. Binding potential

from the liver and the surrounding structures was less than one-tenth that of the portal vein itself, with no significant difference between obese and lean groups ( $V_s = 0.03 \pm 0.005$  vs.  $0.03 \pm 0.001$  mL/cm<sup>3</sup>;  $P = 0.21$ ). The density of portal GLP-1r was substantially less in the obese versus the lean group. In addition to marked differences in the absolute values of the time-activity curves, the plateau of the uptake rate for the portal VOI was about one-half in the obese compared with the lean group (Fig. 2 and Supplementary Fig. 2), so their

**Table 1**—Phenotypic and metabolic characteristics of mini-pigs in the lean and obese groups

	Lean	Obese
Body weight (kg)	$37.2 \pm 1.90$	$85.3 \pm 2.33^*$
Abdominal fat mass (kg)	$3.9 \pm 0.76$	$26.1 \pm 0.93^*$
Visceral fat mass (kg)	$2.5 \pm 1.12$	$10.4 \pm 0.67^*$
Fasting glycemia (mmol/L)	$4.5 \pm 0.15$	$4.8 \pm 0.72$
Metabolized glucose ( $\mu\text{mol/kg/min}$ )	$63.2 \pm 10.95$	$39.2 \pm 4.09^*$
ISI ( $\text{dL/kg} \cdot \text{min}/\mu\text{U/mL} \cdot 1\text{E}3$ )	$6.6 \pm 1.02$	$1.8 \pm 0.12^*$

Data are mean  $\pm$  SEM.  $n = 6$  animals in both groups. Data were obtained during anesthesia. ISI, insulin sensitivity index. \*Indicates a significant difference at  $P < 0.05$ .

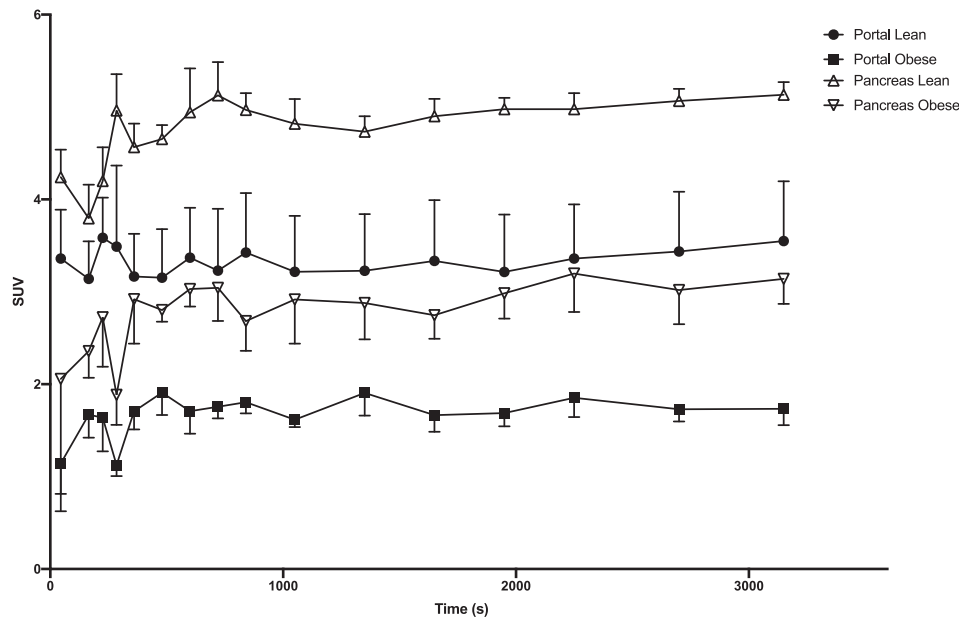


**Figure 2**—Portal and pancreatic time-activity curves in lean and obese animals after the administration of [<sup>68</sup>Ga]Ga-DO3A-VS-Cys40-Exendin-4 at a tracer dose. Data are transformed into standardized uptake values (SUVs) (to quantify the radiotracer concentration in relation to body weight and amount initially injected) to take into account the difference in body weight between groups for representation purposes only. Note the reduction in SUV at the plateau concentration between 15 and 60 min postinjection in both the pancreatic and the portal tissue in the obese vs. lean group. Portal uptake is also consistently less than that in the pancreas. Several time data points (from 0 to 10 min) are not included on the graph to optimize interpretation. Uptake values were obtained from a VOI drawn manually on both injected and noninjected CT images.

binding potentials were also ~50% less in the obese group (Table 2).

In both groups, the uptake data fitted a two-tissue compartment model adequately, which was more acceptable than a single-tissue compartment model, on the basis of both Akaike ( $45 \pm 9$  vs.  $93 \pm 14$  single vs. two compartments for the lean group;  $69 \pm 74$  vs.  $106 \pm 35$  single vs. two compartments for the obese group) and Bayesian information criteria ( $50 \pm 18$  vs.  $91 \pm 18$  single vs. two compartments for the lean group;  $80 \pm 36$  vs.  $76 \pm 45$  single vs. two compartments for the obese group). The reduced binding potential in the obese group was not a consequence of a change in  $k_4$  but rather a decrease by ~80% of  $K_1$  and an ~50% reduction in  $k_3$  transfer

coefficients. Total volume of distribution ( $V_t$ ) followed a parallel change to the  $V_s$ /binding potential value as a consequence of the rapid equilibration of the tracer after its administration. Furthermore, the minute and nonsignificant difference (5.4% and 5.3% for the lean vs. obese group, respectively,  $P > 0.05$ ) between  $V_t$  and  $V_s$  indicated that most of the tracer was in the specific compartment and that repartition was not different between the groups.

Conversion of the dynamic images, combined with high-resolution input function, into  $V_s$ -coded ones allowed the identification of the distribution of the GLP-1r along the path of the portal vein. While slightly noisier than the portal VOI approach, the absolute binding potentials matched those calculated using a compartmental analysis

**Table 2**—Two-tissue compartment model transfer coefficients of [<sup>68</sup>Ga]Ga-DO3A-VS-Cys40-Exendin-4 binding at the portal area

	Lean	Obese
K1 (mL/cm <sup>3</sup> /min)	$1.06 \pm 0.271$	$0.24 \pm 0.051^*$
k2 (L/min)	$5.71 \pm 0.663$	$1.36 \pm 0.065^*$
k3 (L/min)	$0.11 \pm 0.061$	$0.05 \pm 0.021^*$
k4 (L/min)	$0.005 \pm 0.002$	$0.004 \pm 0.003$
Vt (mL/cm <sup>3</sup> )	$4.80 \pm 0.139$	$2.42 \pm 0.074^*$
Vs-BPp (mL/cm <sup>3</sup> )	$4.54 \pm 0.084$	$2.29 \pm 0.167^*$

Data are mean  $\pm$  SE.  $n = 6$  animals in both groups.  $V_t$  and  $V_s$  were calculated according to Innis et al. (68).  $V_s$  indicates the ratio between the volume of distribution within the specifically bound compartment and the plasma concentration and was considered as the primary metric for binding potential. BPp, binding potential of specific tracer binding. \*Indicates a significant difference at  $P < 0.05$ .

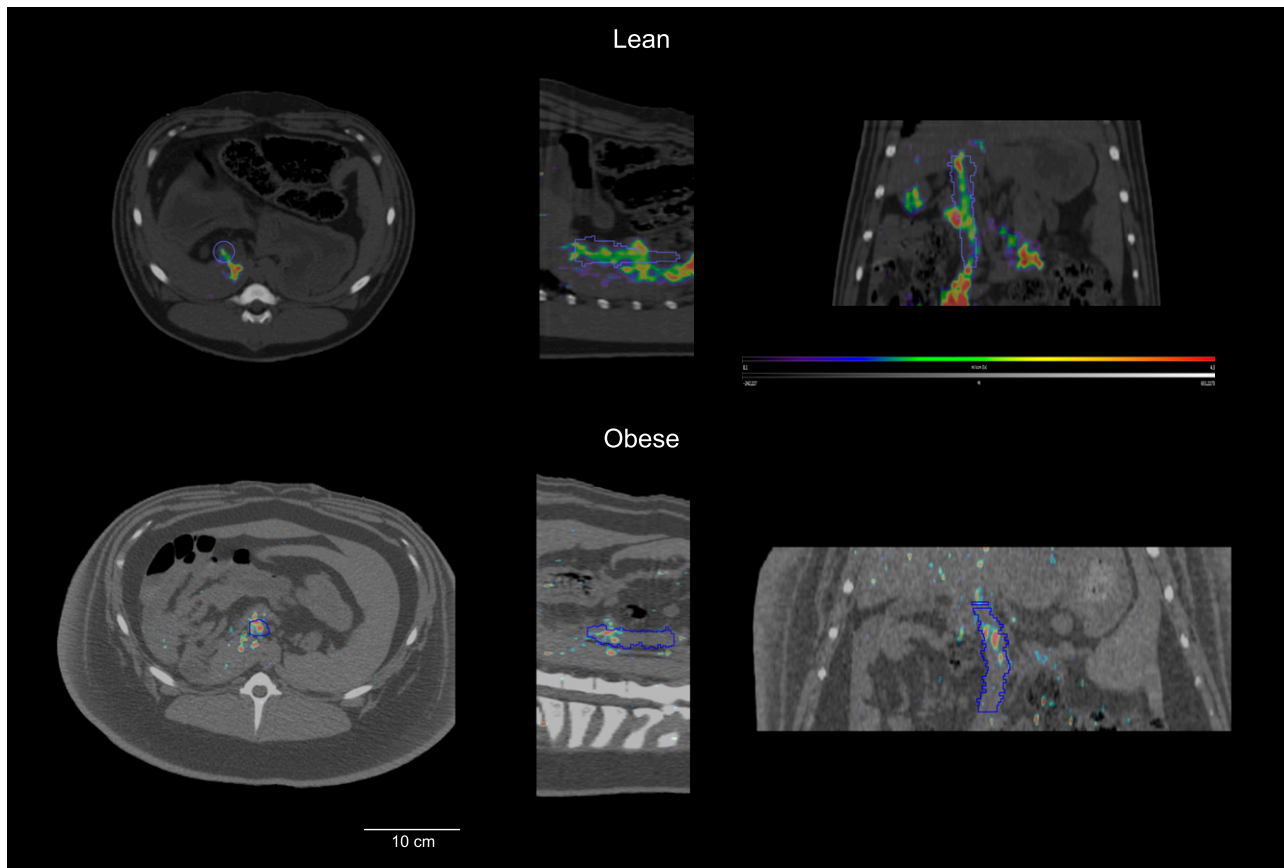


**Figure 3**—Hybrid image representing GLP-1r binding potential (in color scale) coregistered with a noninjected CT image (in grayscale) of the abdomen in lean and obese pigs. The uptake of [ $^{68}\text{Ga}$ ]Ga-DO3A-VS-Cys40-Exendin-4 is represented according to voxelwise Vs coding of the uptake (i.e., the color bar quantifies the density of GLP-1r). The VOI of the portal region is outlined in blue. The position of the section was selected to outline the maximal volume of the VOI without reformatting the images along the portal path. Note the modest binding in the portal area in the obese animal compared with the lean one.

in the lean and obese groups. In the obese group, the portal vein was only weakly visualized using PET imaging only, unlike in the lean group (Fig. 3 and Supplementary Fig. 3). Furthermore, the binding potential along the portal vein did not follow the same anatomical repartition in the two groups (Fig. 1B). In lean animals, the maximal density of GLP-1r was located within the vicinity of the entrance of the portal vein within the liver (porta hepatis), with a relatively constant density between this location and the splenic vein bifurcation followed by a progressive reduction along the path of the superior mesenteric vein. In contrast, in obese animals, there was almost no binding at the porta hepatis level, and the maximum concentration was observed close to the splenic vein bifurcation and to the superior mesenteric vein.

#### Electrophysiological Functional Characterization

Between two and four single-fiber vagal afferents responding to portal field stimulation could be dissected appropriately in each animal. A total of 13 portal afferent neurons in lean and 10 in obese animals were studied. There was no change in arterial glycemia either during or

30 min after the intraportal glucose injection in either the lean or the obese group ( $P > 0.05$ ).

All neurons were of the C type, with a conducting speed of  $1.9 \pm 0.8$  m/s with no significant difference between the two groups ( $P < 0.05$ ) (Supplementary Fig. 4). They were spontaneously active with a mean firing frequency of  $7.1 \pm 4.8$  impulses (imp)/s. No apparent modulation of the instantaneous firing frequency was evident (Fig. 4). Similarly, there were no differences in basal firing rate between the groups ( $7.3 \pm 4.8$  vs.  $6.9 \pm 4.5$  imp/s for the lean vs. obese group,  $P > 0.05$ ). Two neurons, both from the lean group, exhibited periods of total quiescence lasting  $\sim 3$  min and recurring about every 10 min without an apparent cause.

Intraportal glucose infusion reduced the firing rate within  $2.5 \pm 5.3$  min in the lean group but had no significant effect in the obese group. The reduction in firing frequency ranged from total inhibition to 47% of the basal frequency, with a mean inhibition of  $32 \pm 12\%$  at the nadir of the inhibition. Similarly, the time to reach maximal inhibition was also variable, ranging from 8 to 16 min ( $14 \pm 3.9$  min). In contrast, once maximal inhibition was

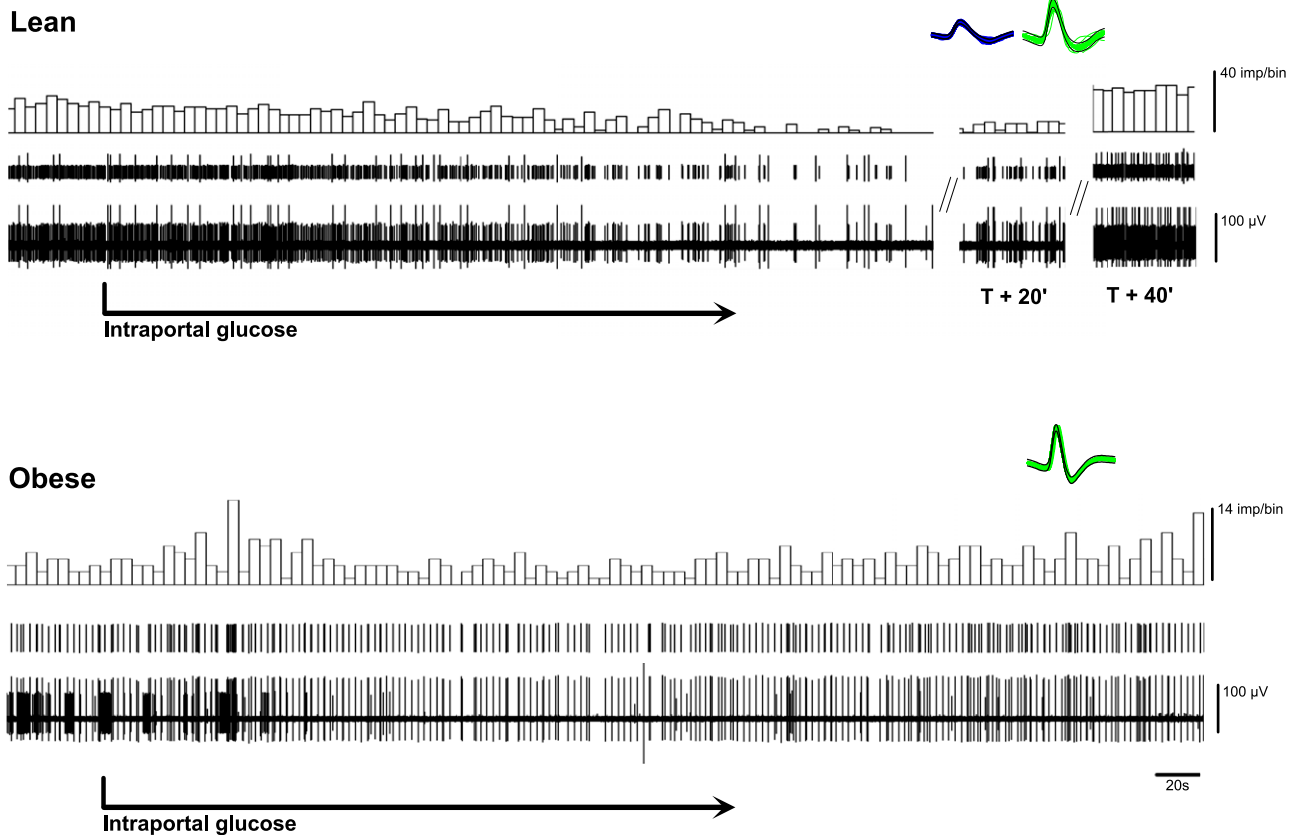


**Figure 4**—Effect of portal administration of glucose on the electrophysiological characteristics of a single-neuron vagal afferent with its free ending located within the portal wall. The figure represents the raw recording, the afferent under scrutiny, and the associated discharge rate summed every 5 s. The inset depicts the template used to discriminate the spikes. Glucose was infused at a rate that was three times the endogenous glucose production rate in the fasted pig (0.045 mL/kg/min of 20% glucose). Note the close-to-total silencing of the vagal afferent 6 min after the onset of the glucose infusion in the lean animal, whereas there was no change in the spiking frequency of the obese animal.

achieved, the return to baseline was similar irrespective of the afferent, and the frequency rate followed an exponential pattern with a half-time of  $8.5 \pm 2.0$  min (Supplementary Fig. 5). Coinjection of glucose and the GLP-1r antagonist Exendin-3 (9-39) was possible as a terminal procedure in all animals, providing information on 46% and 60% of the recorded vagal neurons in the lean and obese groups, respectively. Coinjection of the GLP-1r antagonist suppressed the effect of glucose in the lean group (Fig. 5). The firing rate was unaffected by the coinjection compared with baseline in the obese group ( $P > 0.05$ ).

## DISCUSSION

Using PET imaging with a new positron-emitting probe and single-cell electrophysiological methods linked by image-based abdominal navigation, we have demonstrated in obese, insulin-resistant animals that the function of the portal vagal glucose sensor is disordered such that portal glucose, within the concentrations likely to occur after a meal, is not detected. This insensitivity of vagal afferents to glucose in obese, insulin-resistant, but not lean, animals appears to be a consequence of a reduced portal GLP-1r

density, especially between the porta hepatis and the left gastric vein, a feature further demonstrated by the suppression of the glucose effect on the afferent by pharmacological inhibition of GLP-1r in lean animals only. Because of difficulties in identifying the portal sensor, previous studies have focused on the physiological consequences of sensor activation. Therefore, information relating to portal sensor behavior in insulin-resistant obesity has, hitherto, been limited (24).

Recently, a study from the D'Alessio group in the rat (45), where there is evidence for hepatportal GLP-1 sensing (9), did not support portal-specific signaling during GLP-1 infusion. A higher insulinotropic effect was observed after jugular versus portal GLP-1 injection, which was not affected by dipeptidyl peptidase 4 inhibition. The observations in this study, which used relatively high doses of GLP-1 and glucose, are contrary to those of several other groups (8,14,46). In our study, we used a dose of glucose that is within the range of the endogenous glucose quantified precisely by fluorodeoxyglucose uptake for animals of the same weight and identical age (31,47). Depending on the putative portal detection system, which is unknown

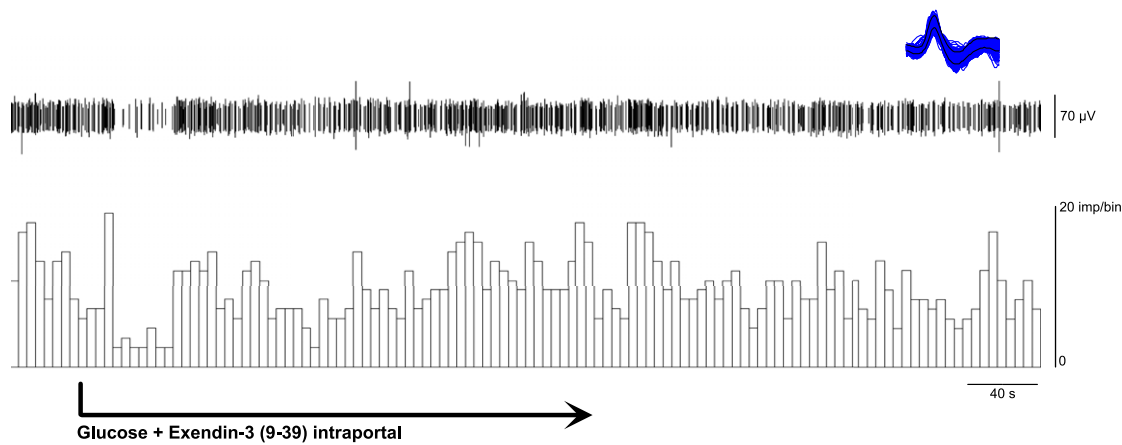


**Figure 5**—Effect of coinfusion of glucose with a GLP-1r antagonist on the electrophysiological characteristics of a single-neuron vagal afferent with its free ending located within the portal wall. Exendin-3 (9-39), a GLP-1r antagonist, completely blunted the inhibitory effect of intraportal glucose in the lean animals. The graph represents the spike under scrutiny together with its discharge rate. The inset is the template used for spike detection.

at present (e.g., SGLT3 with  $K_m$  close to basal glycemia vs. GLUT2 with  $K_m$  four times larger), the interpretation of the outcomes of studies using large ranges in glucose infusion varies (1). Our observations support an alternative, yet not incompatible, explanation reflecting the uneven distribution of the GLP-1r along the portal vein. We demonstrated that the GLP-1r-rich segment of the portal vein is short—a few centimeters even in a large animal—and that in lean animals, GLP-1r density rapidly increased after the splenic vein confluent. Therefore, it would not be surprising if very small changes in the location of the tip of the portal catheter resulted in marked modifications in the intensity of the afferent signal, grossly proportional to the density of activated receptor. Furthermore, the hepatoportal area, being attached directly to the hepatic ligament, moves with a gross amplitude close to that of the diaphragm, an artifact that can be accounted for partially using imaging methods (48) but is inaccessible with an implanted catheter. Finally, it is recognized that the anatomy of this portal segment is highly variable across individuals and breeds (49,50).

Given the controversy relating the potential preeminence of a peripheral versus central glucose detector (51) together with the probability of dual incongruent hypoglycemic versus hyperglycemic detectors (1,45), our approach was not designed to improve understanding of the central detection site. Indeed,  $^{68}\text{Ga-DO3A}$  and  $^{68}\text{Ga-DOTA}$  derivatives are unable to cross the brain-blood barrier (52), the maximal transport being  $\sim 5\%$ , which is inadequate to perform receptor binding studies. Similarly, we have not evaluated the response of the portal vein to hypoglycemia given pervasive evidence that the neural network involved in this detection is primarily, if not exclusively, mediated by spinal afferents (7).

To our knowledge, this is the first study in which nervous afferent targeting has been performed in vivo

using PET imaging coupled with image-based navigation. This approach allows the stimulating electrodes to be inserted at the location where GLP-1r is maximal, optimizing the capacity to identify GLP-1r-responsive portal vagal afferent neurons. This strategy, while being complex, has major advantages compared with vagal recording from the sectioned hepatic branch or ex vivo recording (13,36,53), which hitherto represents the only direct report of portal vagal afferent activity. Because the recording is performed at the cervical level, prolonged recording of a true single afferent is feasible, even in obese animals in contrast to the mass recording of the entire hepatic bundle hitherto achieved. It is also not necessary to section the contralateral cervical vagus. Because of the bilateral organization of the vagus (54), this strategy preserves, albeit incompletely, the integrity of the efferent limb of the vagus, which is important in glucose homeostasis (55,56). Our vagal recordings were also performed while interaction with the abdominal organs was minimal and in a closed abdomen so that the afferents remained in their usual anatomical location. Finally, we were able to elicit evoked potentials without insurmountable interference of the stimulation artifact because of the substantial distance between the recording and the stimulation sites.

A previous report, which was based on electrophysiological evidence, described both a decrease (13) and an increase (36) of the overall firing rate of the hepatic branch of the vagus in rats and guinea pigs during portal glucose infusion. In contrast, we consistently observed a decreased firing rate of a single-neuron portal vagal afferent during glucose infusion. This confirms the observations in mice with targeted inactivation (i.e., inhibition) of GLP-1r in autonomic neurons through *Phox2b*, resulting in impaired glucose homeostasis and hyperinsulinemia (51). Furthermore, several elements could explain these differences to the outcomes of studies. Nijima and colleagues (13,36)

recorded the entire vagal bundle encompassing several neurons resulting in a complex signal, potentially blunting individual neuronal behavior, while we recorded a single-cell afferent that responded without dampening to the chemical environment of its endings. Furthermore, the actual area of the vagal endings could not be inferred from the recordings by Nijima and colleagues because the hepatic branch of the vagus innervates not only the portal vein but also part of the pancreas, the duodenum, and the liver itself. The localization of the vagal neuron endings by field stimulation, while imperfect, is nevertheless precise. The electronic spread occurring during field stimulation could be modeled using finite element method equations (see Supplementary Material), and the probability of “en passant” stimulation of the gastroduodenal branch is extremely low. We could have selected a subpopulation of vagal afferents acting through the GLP-1r using the GLP-1r map to locate the stimulating electrodes on a specific portal area and appreciate that another location might have resulted in a different vagal firing rate. The suppression of the glucose-induced inhibition by the coinjection of a GLP-1r antagonist established that the neurons targeted by our strategy are primarily GLP-1 sensitive.

The observed change in the distribution of GLP-1r along the portal vein induced by obesity is novel and likely to be important: There was a low density of receptors between the porta hepatis and the left gastric vein in the obese animals in contrast to the high density in the lean animals. A probable consequence of this anatomical arrangement is that the glucose derived from venous supplies flowing above the splenic vein will be detected less in the obese animals. This would include venous blood not only from the stomach but also from the superior duodenopancreatic vein that branched at the same level as the gastric veins (Supplementary Fig. 6). While the supply from the gastric vein is unlikely to be of major physiological relevance, given the inability of the stomach to absorb glucose (57), the input of the duodenopancreatic vein, while not identifiable in all animals, may be important because GLP-1 secreted by pancreatic  $\alpha$ -cells (58) reached the circulation through this vein (Supplementary Fig. 6). Furthermore, the GLP-1r has been demonstrated in  $\alpha$ -cells (59), where it feeds an autocrine loop (60). A smaller amount of GLP-1 also originates from the mesenteric vein, but because of its very rapid degradation, only a small fraction of L-cell intestinal secretion reaches the portal sensor (61). Therefore, in lean animals, the main source of GLP-1 for the portal sensor is almost certainly the area of GLP-1r maximal density (i.e., between the porta hepatis and the gastric veins/duodenopancreatic vein). This is consistent with our observation that this is the area, in obese animals, that exhibits a lower amount of GLP-1r.

The similarity between Vt values obtained from spectral analysis versus two-compartmental fitting suggested that a two-tissue compartment model was preferable to a one-tissue model to fit the experimental data (see Supplementary Material). This represented a difference from the

one-tissue compartment model used formerly (37), which is likely to be attributable to differences in the input arterial function measurement. The Eriksson group used discrete sampling of venous blood (62), whereas we used online measurement of the arterial radioactivity. Nevertheless, the biological meaning of the two compartments can only be hypothesized on the basis of a priori knowledge of the ligand behavior (63) together with general principles established for the brain ligands (64). We are confident that the model does not require metabolite correction since  $^{68}\text{Ga}$ -DO3A-Exendin-4 has been shown to be stable for several hours after injection (65). The possibility of an irreversible compartment, such as that described for another Exendin  $^{68}\text{Ga}$  tracer for rat myocardium (66), cannot be excluded, but small variations in the linker molecule attached to Exendin result in large variations in the internalization (67). However, internalization capabilities of  $^{68}\text{Ga}$ -DO3A-Exendin-4 at the portal area are unknown.

Our study has several limitations inherent in the intricacies of the *in vivo* quantification of GLP-1r. The V<sub>s</sub>-binding potential is not an absolute measurement of the receptor density, and while we measured receptor concentration, imaging at multiple specific activities is a prerequisite for calculation of the total available receptor concentration (68). This allows for variations in the occupancy of the receptor by the radioligand (69). The specificity of [ $^{68}\text{Ga}$ ]Ga-DO3A-VS-Cys40-Exendin-4 binding on portal GLP-1r may be less than desirable, especially in a porcine model. Previous studies on the pancreas of growing juvenile pigs suggested that pancreatic uptake of [ $^{68}\text{Ga}$ ]Ga-DO3A-VS-Cys40-Exendin-4 is unrelated to the number of  $\beta$ -cells (62) since the marked reduction in  $\beta$ -cells induced by streptozotocin is not in proportion to the reduction in radioactive uptake within the pancreatic area. Nevertheless, irrespective of the cellular localization of the GLP-1r labeled within the pancreas, our data support the specificity of the radioactive tracer on portal GLP-1r. Such specificity is not surprising given that activation of the hepatoportal sensor after the injection of Exendin-4 in dogs has been demonstrated (10). It may be considered surprising that the outer boundaries of the portal vein were equally radioactive compared with the inner part of the vein. Part of the radioactivity observed within the vessel could be due to the radioligand binding to blood proteins. However, this is unlikely since both above and below the portal VOI, the amount of radioactivity within the vessel is extremely small. A more likely explanation is the limited spatial resolution of the PET image.

While we conducted a quantitative assessment of GLP-1r density, the method is unable to discriminate down-regulation of the number of GLP-1rs per unit of volume from a reduced affinity of Exendin-4 toward its natural receptor. Absolute affinity could be quantitatively measured through PET measurements since affinity is the ratio between binding potential and total receptor density (68). Unfortunately, calculating total receptor density requires incremental doses of the cold ligand that would have been

likely to markedly reduce the survival of animals as a consequence of induced hypoglycemia and cardiac dysfunction (62). Since our goal was to use PET receptor mapping to localize the portal sensor for subsequent electrophysiological measurements, this was considered, a priori, to be an unacceptable risk that could also impair the quality of the raw data.

The overall reduction in binding potential, together with the modifications in the spatial arrangement of GLP-1r in the obese group, may be relevant to an understanding of the reduced incretin effect in type 2 diabetes (70). Chemical portal denervation in dogs affects oral glucose tolerance, with plasma glucose and insulin responses being 50% higher postdenervation (10). It could be speculated that the suppression of GLP-1r-related glucose sensing observed in the obese group has similarities to that observed in portal denervated dogs and, conversely, that obesity functionally denervates the portal sensor through altered GLP-1 sensing. The observed absence of changes in the firing rate of portal vagal afferents in response to glucose infusion supports this concept by providing the functional counterpart of the receptor mapping alteration evident in the obese group. Prior studies using denervation of the portal area, with and without denervation of the liver, failed to identify the precise location of the sensor and with an inference that part, if not all, is within the liver (71). Our observations argue strongly against the possibility of an intrahepatic sensor since the binding potential of the liver was, at most, one-tenth of that of the portal vein.

Thorens (24) suggested in 2008 that deregulation of the peripheral glucose sensors may be important in obesity and type 2 diabetes because peripheral glucose sensors control physiological functions, which when deregulated, trigger mechanisms relevant to the pathogenesis of obesity and diabetes. Until now, the majority, if not all, of the data related to the portal sensor was the outcome of indirect experimental techniques (e.g., altered peripheral glucose uptake [72], impairment in the first phase of insulin secretion [73]). The importance of the GLP-1r-dependent portal sensor to some of these indirect effects has also been challenged, particularly the reduction in food intake (18). In the current study, we confirm that some of these associations are likely to reflect defective portal glucose sensing in the insulin-resistant obese. Understanding the roles of different GLP-1-responsive neurons is very important because therapeutic strategies that involve mimicry or stabilization of GLP-1 provide clinically important approaches for the management of diabetes and, potentially, other metabolic disorders. However, there is a substantial interindividual variation in the magnitude of the therapeutic response, and the absence of factors hitherto identified to indicate which patients will respond best to these drugs (74) attests to the need for minimally invasive tools, such as the one described here, to improve patient management in a personalized medicine perspective.

In conclusion, we have demonstrated that in the pig, obesity-induced insulin resistance leads to functional

portal denervation with a marked suppression of vagal sensitivity to portal glucose. The latter appears to be the consequence of a reduction in the density of portal GLP-1r, as indicated by diminished GLP-1r binding potential in obese, insulin-resistant animals.

**Acknowledgments.** The authors thank the staff of the UEPR Unit, INRAE, for animal care: Mickael Genissel, Julien Georges, Francis Le Gouevic, and Vincent Piedvache. The authors also thank Emilie Lebrun and Laurine Piquemal (Aniscan Unit, INRAE) for involvement in running the Aniscan imaging and Raphael Comte (Pegase Unit, INRAE) for insulin measurements. Furthermore, the authors thank Eric Bobillier of INRAE for the development of the single-unit preamplifier device.

**Funding.** The study was conducted within the Aniscan Imaging Center (Aniscan, INRAE), which is supported by BPI France within the Investments for the Future program. K.L.J.'s salary is supported by The University of Adelaide William T. Southcott Research Fellowship.

**Duality of Interest.** No potential conflicts of interest relevant to this article were reported.

**Author Contributions.** C.-H.M. planned the experiments, conducted the studies, analyzed the data, and was primarily responsible for writing the manuscript. A.C. conducted the studies and analyzed the data. M.H. and K.L.J. made a major contribution to the writing of the manuscript, including data interpretation. C.-H.M. is the guarantor of this work and, as such, had full access to all the data in the study and takes responsibility for the integrity of the data and the accuracy of the data analysis.

## References

- Soty M, Gautier-Stein A, Rajas F, Mithieux G. Gut-brain glucose signaling in energy homeostasis. *Cell Metab* 2017;25:1231–1242
- Sandoval D, Cota D, Seeley RJ. The integrative role of CNS fuel-sensing mechanisms in energy balance and glucose regulation. *Annu Rev Physiol* 2008;70:513–535
- Pal A, Rhoads DB, Tavakkoli A. Effect of portal glucose sensing on systemic glucose levels in SD and ZDF rats. *PLoS One* 2016;11:e0165592
- Berthoud HR. Anatomy and function of sensory hepatic nerves. *Anat Rec A Discov Mol Cell Evol Biol* 2004;280:827–835
- Mithieux G. Détection du glucose sanguin par le système nerveux: pourquoi, où, comment? *Ann Biol Clin (Paris)* 2020;78:134–138 [in French]
- Matveyenko AV, Donovan CM. Metabolic sensors mediate hypoglycemic detection at the portal vein. *Diabetes* 2006;55:1276–1282
- Bohland M, Matveyenko AV, Saberi M, Khan AM, Watts AG, Donovan CM. Activation of hindbrain neurons is mediated by portal-mesenteric vein glucose-sensors during slow-onset hypoglycemia. *Diabetes* 2014;63:2866–2875
- Balkan B, Li X. Portal GLP-1 administration in rats augments the insulin response to glucose via neuronal mechanisms. *Am J Physiol Regul Integr Comp Physiol* 2000;279:R1449–R1454
- Vahl TP, Tauchi M, Durler TS, et al. Glucagon-like peptide-1 (GLP-1) receptors expressed on nerve terminals in the portal vein mediate the effects of endogenous GLP-1 on glucose tolerance in rats. *Endocrinology* 2007;148:4965–4973
- Ionut V, Castro AVB, Woolcott OO, et al. Hepatic portal vein denervation impairs oral glucose tolerance but not exenatide's effect on glycemia. *Am J Physiol Endocrinol Metab* 2014;307:E644–E652
- Bai L, Mesgarzadeh S, Ramesh KS, et al. Genetic identification of vagal sensory neurons that control feeding. *Cell* 2019;179:1129–1143.e23
- Nijima A. Glucose-sensitive afferent nerve fibres in the hepatic branch of the vagus nerve in the Guinea-pig. *J Physiol* 1982;332:315–323
- Nijima A, Torii K, Uneyama H. Role played by vagal chemical sensors in the hepato-portal region and duodeno-intestinal canal: an electrophysiological study. *Chem Senses* 2005;30(Suppl. 1):i178–i179

14. Nishizawa M, Nakabayashi H, Uehara K, Nakagawa A, Uchida K, Koya D. Intraportal GLP-1 stimulates insulin secretion predominantly through the hepatoportal-pancreatic vagal reflex pathways. *Am J Physiol Endocrinol Metab* 2013; 305:E376–E387
15. Berthoud H-R, Neuhuber WL. Functional and chemical anatomy of the afferent vagal system. *Auton Neurosci* 2000;85:1–17
16. Burcelin R, Da Costa A, Drucker D, Thorens B. Glucose competence of the hepatoportal vein sensor requires the presence of an activated glucagon-like peptide-1 receptor. *Diabetes* 2001;50:1720–1728
17. Krieger JP, Arnold M, Pettersen KG, Lossel P, Langhans W, Lee SJ. Knockdown of GLP-1 receptors in vagal afferents affects normal food intake and glycemia. *Diabetes* 2016;65:34–43
18. Müller TD, Finan B, Bloom SR, et al. Glucagon-like peptide 1 (GLP-1). *Mol Metab* 2019;30:72–130
19. Burcelin R. The incretins: a link between nutrients and well-being. *Br J Nutr* 2005;93(Suppl. 1):S147–S156
20. Waser B, Blank A, Karamitopoulou E, Perren A, Reubi JC. Glucagon-like-peptide-1 receptor expression in normal and diseased human thyroid and pancreas. *Mod Pathol* 2015;28:391–402
21. Gray SM, Xin Y, Ross EC, et al. Discordance between GLP-1R gene and protein expression in mouse pancreatic islet cells. *J Biol Chem* 2020;295:11529–11541
22. Broide E, Bloch O, Ben-Yehudah G, Cantrell D, Shirin H, Rapoport MJ. Reduced GLP-1R expression in gastric glands of patients with type 2 diabetes mellitus. *J Clin Endocrinol Metab* 2014;99:E1691–E1695
23. Duca FA, Sakar Y, Covasa M. Combination of obesity and high-fat feeding diminishes sensitivity to GLP-1R agonist exendin-4. *Diabetes* 2013;62:2410–2415
24. Thorens B. Glucose sensing and the pathogenesis of obesity and type 2 diabetes. *Int J Obes* 2008;32(Suppl. 6):S62–S71
25. Selvaraju RK, Velikyan I, Asplund V, et al. Pre-clinical evaluation of [(68)Ga] Ga-D03A-VS-Cys(40)-Exendin-4 for imaging of insulinoma. *Nucl Med Biol* 2014; 41:471–476
26. Velikyan I, Rosenstrom U, Eriksson O. Fully automated GMP production of [(68)Ga]Ga-D03A-VS-Cys(40)-Exendin-4 for clinical use. *Am J Nucl Med Mol Imaging* 2017;7:111–125
27. Pyke C, Knudsen LB. The glucagon-like peptide-1 receptor—or not? *Endocrinology* 2013;154:4–8
28. Cuche G, Blat S, Malbert CH. Desensitization of ileal vagal receptors by short-chain fatty acids in pigs. *Am J Physiol Gastrointest Liver Physiol* 2001;280:G1013–G1021
29. Malbert CH, Bobillier E, Picq C, Divoux JL, Guiraud D, Henry C. Effects of chronic abdominal vagal stimulation of small-diameter neurons on brain metabolism and food intake. *Brain Stimul* 2017;10:735–743
30. Nishizawa M, Nakabayashi H, Kawai K, et al. The hepatic vagal reception of intraportal GLP-1 is via receptor different from the pancreatic GLP-1 receptor. *J Auton Nerv Syst* 2000;80:14–21
31. Bahri S, Horowitz M, Malbert CH. Inward glucose transfer accounts for insulin-dependent increase in brain glucose metabolism associated with diet-induced obesity. *Obesity (Silver Spring)* 2018;26:1322–1331
32. Sauleau P, Lapouble E, Val-Laillet D, Malbert CH. The pig model in brain imaging and neurosurgery. *Animal* 2009;3:1138–1151
33. Askeland C, Solberg OV, Bakeng JBL, et al. CustusX: an open-source research platform for image-guided therapy. *Int J CARS* 2016;11:505–519
34. Eriksson O, Rosenström U, Selvaraju RK, Eriksson B, Velikyan I. Species differences in pancreatic binding of D03A-VS-Cys(40)-Exendin4. *Acta Diabetol* 2017;54:1039–1045
35. Malbert C-H, Horowitz M, Young RL. Low-calorie sweeteners augment tissue-specific insulin sensitivity in a large animal model of obesity. *Eur J Nucl Med Mol Imaging* 2019;46:2380–2391
36. Nijijima A, Mei N. Glucose sensors in viscera and control of blood glucose level. *Physiology (Bethesda)* 1987;2:164–167
37. Selvaraju RK, Velikyan I, Johansson L, et al. In vivo imaging of the glucagon-like peptide 1 receptor in the pancreas with <sup>68</sup>Ga-labeled D03A-exendin-4. *J Nucl Med* 2013;54:1458–1463
38. Malbert C-H. AniMate-An open source software for absolute PET quantification. In *Annual Congress of the European Association of Nuclear Medicine*. Vol. 43, 2016
39. Bettinardi V, Castiglioni I, De Bernardi E, Gilardi MC. PET quantification: strategies for partial volume correction. *Clin Transl Imaging* 2014;2:199–218
40. Plonsey R, Barr RC. Electric field stimulation of excitable tissue. *IEEE Eng Med Biol Mag* 1998;17:130–137
41. Mei N, Condamine M, Boyer A. The composition of the vagus nerve of the cat. *Cell Tissue Res* 1980;209:423–431
42. Dai M, Picq C, Rossel O, Maciejasz P, Malbert CH, Guiraud D. Comparison of the efficiency of chopped and non-rectangular electrical stimulus waveforms in activating small vagus nerve fibers. *J Neurosci Methods* 2019;320:1–8
43. Malbert CH, Picq C, Divoux J-L, Henry C. Bilateral stimulation of the abdominal vagus modifies dopamine connectivity in acquired obesity. *Eur J Nucl Med Mol Imaging* 2017;44:S588
44. Nielsen MF, Roelsgaard K, Keiding S, et al. Impaired hepatic counter-regulatory response to insulin-induced hypoglycemia in hepatic denervated pigs. *J Clin Transl Endocrinol* 2015;2:131–136
45. Aulinger BA, Perabo M, Seeley RJ, Parhofer KG, D'Alessio DA. Rapid hepatic metabolism blunts the endocrine action of portally infused GLP-1 in male rats. *Am J Physiol Endocrinol Metab* 2020;318:E189–E197
46. Ahrén B. Sensory nerves contribute to insulin secretion by glucagon-like peptide-1 in mice. *Am J Physiol Regul Integr Comp Physiol* 2004;286:R269–R272
47. Malbert C-H, Picq C, Divoux J-L, Henry C, Horowitz M. Obesity-associated alterations in glucose metabolism are reversed by chronic bilateral stimulation of the abdominal vagus nerve. *Diabetes* 2017;66:848–857
48. Lu Y, Fontaine K, Mulnix T, et al. Respiratory motion compensation for PET/CT with motion information derived from matched attenuation-corrected gated PET data. *J Nucl Med* 2018;59:1480–1486
49. van Leeuwen MS, Noordzij J, Fernandez MA, Hennipman A, Feldberg MA, Dillon EH. Portal venous and segmental anatomy of the right hemiliver: observations based on three-dimensional spiral CT renderings. *AJR Am J Roentgenol* 1994;163:1395–1404
50. Bekheit M, Bucur PO, Wartenberg M, Vibert E. Computerized tomography-based anatomic description of the porcine liver. *J Surg Res* 2017;210:223–230
51. Varin EM, Mulvihill EE, Baggio LL, et al. Distinct neural sites of GLP-1R expression mediate physiological versus pharmacological control of incretin action. *Cell Rep* 2019;27:3371–3384.e3
52. Martiniova L, Palatis L, Etchebehere E, Ravizzini G. Gallium-68 in medical imaging. *Curr Radiopharm* 2016;9:187–207
53. Nakabayashi H, Nishizawa M, Nakagawa A, Takeda R, Nijijima A. Vagal hepatopancreatic reflex effect evoked by intraportal appearance of tGLP-1. *Am J Physiol* 1996;271:E808–E813
54. Guiraud D, Andreu D, Bonnet S, et al. Vagus nerve stimulation: state of the art of stimulation and recording strategies to address autonomic function neuro-modulation. *J Neural Eng* 2016;13:041002
55. Lee KC, Miller RE. The hepatic vagus nerve and the neural regulation of insulin secretion. *Endocrinology* 1985;117:307–314
56. Shikora S, Toulli J, Herrera MF, et al. Vagal blocking improves glycemic control and elevated blood pressure in obese subjects with type 2 diabetes mellitus. *J Obes* 2013;2013:245683
57. Maddock SJ, Trimble HC, Carey BW Jr. Is d-glucose absorbed from the stomach of the dog? *J Biol Chem* 1933;103:285–294
58. Paternoster S, Falasca M. Dissecting the physiology and pathophysiology of glucagon-like peptide-1. *Front Endocrinol (Lausanne)* 2018;9:584
59. Heller RS, Kieffer TJ, Habener JF. Insulinotropic glucagon-like peptide 1 receptor expression in glucagon-producing  $\alpha$ -cells of the rat endocrine pancreas. *Diabetes* 1997;46:785–791

60. Piro S, Mascali LG, Urbano F, et al. Chronic exposure to GLP-1 increases GLP-1 synthesis and release in a pancreatic alpha cell line ( $\alpha$ -TC1): evidence of a direct effect of GLP-1 on pancreatic alpha cells. *PLoS One* 2014;9:e90093
61. D'Alessio D. Is GLP-1 a hormone: whether and when? *J Diabetes Investig* 2016;7(Suppl. 1):50–55
62. Nalin L, Selvaraju RK, Velikyan I, et al. Positron emission tomography imaging of the glucagon-like peptide-1 receptor in healthy and streptozotocin-induced diabetic pigs. *Eur J Nucl Med Mol Imaging* 2014;41:1800–1810
63. Wild D, Wicki A, Mansi R, et al. Exendin-4-based radiopharmaceuticals for glucagonlike peptide-1 receptor PET/CT and SPECT/CT. *J Nucl Med* 2010;51:1059–1067
64. Hong YT, Fryer TD. Kinetic modelling using basis functions derived from two-tissue compartmental models with a plasma input function: general principle and application to [ $^{18}$ F]fluorodeoxyglucose positron emission tomography. *Neuroimage* 2010;51:164–172
65. Selvaraju RK, Bulenga TN, Espes D, et al. Dosimetry of [(68)Ga]Ga-DO3A-VS-Cys(40)-Exendin-4 in rodents, pigs, non-human primates and human - repeated scanning in human is possible. *Am J Nucl Med Mol Imaging* 2015;5:259–269
66. Ståhle M, Kytö V, Kiugel M, et al. Glucagon-like peptide-1 receptor expression after myocardial infarction: imaging study using  $^{68}$ Ga-NODAGA-exendin-4 positron emission tomography. *J Nucl Cardiol*, 13 December 2018. Available from <https://doi.org/10.1007/s12350-018-01547-1>
67. Jodal A, Lankat-Buttgereit B, Brom M, Schibli R, Béhé M. A comparison of three (67/68)Ga-labelled exendin-4 derivatives for  $\beta$ -cell imaging on the GLP-1 receptor: the influence of the conjugation site of NODAGA as chelator. *EJNMMI Res* 2014;4:31
68. Innis RB, Cunningham VJ, Delforge J, et al. Consensus nomenclature for in vivo imaging of reversibly binding radioligands. *J Cereb Blood Flow Metab* 2007; 27:1533–1539
69. Zhang Y, Fox GB. PET imaging for receptor occupancy: meditations on calculation and simplification. *J Biomed Res* 2012;26:69–76
70. Herzberg-Schäfer S, Heni M, Stefan N, Häring HU, Fritsche A. Impairment of GLP1-induced insulin secretion: role of genetic background, insulin resistance and hyperglycaemia. *Diabetes Obes Metab* 2012;14(Suppl. 3):85–90
71. Pagliassotti MJ, Tarumi C, Neal DW, Cherrington AD. Hepatic denervation alters the disposition of an enteral glucose load in conscious dogs. *J Nutr* 1991; 121:1255–1261
72. Burcelin R, Dolci W, Thorens B. Portal glucose infusion in the mouse induces hypoglycemia: evidence that the hepatportal glucose sensor stimulates glucose utilization. *Diabetes* 2000;49:1635–1642
73. Preitner F, Ibberson M, Franklin I, et al. Gluco-incretins control insulin secretion at multiple levels as revealed in mice lacking GLP-1 and GIP receptors. *J Clin Invest* 2004;113:635–645
74. Monami M, Dicembrini I, Nreu B, Andreozzi F, Sesti G, Mannucci E. Predictors of response to glucagon-like peptide-1 receptor agonists: a meta-analysis and systematic review of randomized controlled trials. *Acta Diabetol* 2017;54:1101–1114